Neurobiology of Disease

# β1-C121W Is Down But Not Out: Epilepsy-Associated *Scn1b-C121W* Results in a Deleterious Gain-of-Function

**Larisa C. Kruger,[1] Heather A. O'Malley,[1] Jacob M. Hull,[1,2] Amanda Kleeman,[1] Gustavo A. Patino,[1] and Lori L. Isom[1,2]**
[1]Department of Pharmacology and [2]Neuroscience Program, University of Michigan, Ann Arbor, Michigan 48109

Voltage-gated sodium channel (VGSC) β subunits signal through multiple pathways on multiple time scales. In addition to modulating sodium and potassium currents, β subunits play nonconducting roles as cell adhesion molecules, which allow them to function in cell–cell communication, neuronal migration, neurite outgrowth, neuronal pathfinding, and axonal fasciculation. Mutations in *SCN1B*, encoding VGSC β1 and β1B, are associated with epilepsy. Autosomal-dominant *SCN1B-C121W*, the first epilepsy-associated VGSC mutation identified, results in genetic epilepsy with febrile seizures plus (GEFS+). This mutation has been shown to disrupt both the sodium-current-modulatory and cell-adhesive functions of β1 subunits expressed in heterologous systems. The goal of this study was to compare mice heterozygous for *Scn1b-C121W* (*Scn1b*$^{+/W}$) with mice heterozygous for the *Scn1b-null* allele (*Scn1b*$^{+/-}$) to determine whether the C121W mutation results in loss-of-function *in vivo*. We found that *Scn1b*$^{+/W}$ mice were more susceptible than *Scn1b*$^{+/-}$ and *Scn1b*$^{+/+}$ mice to hyperthermia-induced convulsions, a model of pediatric febrile seizures. β1-C121W subunits are expressed at the neuronal cell surface *in vivo*. However, despite this, β1-C121W polypeptides are incompletely glycosylated and do not associate with VGSC α subunits in the brain. β1-C121W subcellular localization is restricted to neuronal cell bodies and is not detected at axon initial segments in the cortex or cerebellum or at optic nerve nodes of Ranvier of *Scn1b*$^{W/W}$ mice. These data, together with our previous results showing that β1-C121W cannot participate in *trans*-homophilic cell adhesion, lead to the hypothesis that *SCN1B-C121W* confers a deleterious gain-of-function in human GEFS+ patients.

*Key words:* axon; beta subunit; cell adhesion; epilepsy; febrile seizure; sodium channel

**Significance Statement**

The mechanisms underlying genetic epilepsy syndromes are poorly understood. Closing this gap in knowledge is essential to the development of new medicines to treat epilepsy. We have used mouse models to understand the mechanism of a mutation in the sodium channel gene *SCN1B* linked to genetic epilepsy with febrile seizures plus. We report that sodium channel β1 subunit proteins encoded by this mutant gene are expressed at the surface of neuronal cell bodies; however, they do not associate with the ion channel complex nor are they transported to areas of the axon that are critical for proper neuronal firing. We conclude that this disease-causing mutation is not simply a loss-of-function, but instead results in a deleterious gain-of-function in the brain.

## Introduction

Voltage-gated sodium channels (VGSCs), which are composed of one pore-forming α subunit and two β subunits in the brain (Hartshorne and Catterall, 1981), are critical for neuronal excitability, including action potential (AP) initiation and conduction. Although VGSC β subunits do not form the ion-conducting pore, they are essential for normal excitability *in vivo* through modulation of sodium and potassium currents (Isom et al., 1992; Isom et al., 1995b; Chen et al., 2004; Marionneau et al., 2012). In addition, β subunits are Ig superfamily cell adhesion molecules that play important roles in cell–cell communication, neuronal proliferation and migration, neurite outgrowth, neuronal pathfinding, and axonal fasciculation *in vitro* and *in vivo* (Davis et al., 2004; Brackenbury and Isom, 2008; Patino and Isom, 2010; Brackenbury and Isom, 2011; Patino et al., 2011).

Mutations in VGSC genes are associated with multiple genetic epilepsies, including genetic epilepsy with febrile seizures plus (GEFS+) (Scheffer and Berkovic, 1997; Wallace et al., 1998; Singh et al., 1999) and Dravet syndrome (Patino et al., 2009). Autosomal-dominant mutations in *SCN1B*, encoding VGSC β1 and β1B, are associated with GEFS+ (Wallace et al., 1998; Wal-

Received Jan. 26, 2016; revised May 2, 2016; accepted May 3, 2016.

Author contributions: L.C.K., H.A.O., J.M.H., G.A.P., and L.L.I. designed research; L.C.K., H.A.O., J.M.H., A.K., and G.A.P. performed research; L.C.K. and H.A.O. analyzed data; L.C.K., H.A.O., and L.L.I. wrote the paper.

This work was supported by the National Institutes of Health (Grant R01 NS-076752 to L.L.I., Training Grant T32 GM07544 to L.C.K., and Training Grant T32 GM008322 to J.M.H.), the American Epilepsy Society/Epilepsy Foundation (Predoctoral Fellowship to L.C.K.), the PhRMA Foundation (Predoctoral Fellowship to L.C.K.), and the University of Michigan MiBrain Initiative (Predoctoral Fellowship to J.M.H.).

G.A. Patino's present address: Oakland University William Beaumont School of Medicine, Rochester, MI 48309.

Correspondence should be addressed to Lori L. Isom, Department of Pharmacology, University of Michigan Medical School, 1301 MSRB III, 1150 W. Medical Center Dr., Ann Arbor, MI 48109. E-mail: lisom@umich.edu.

DOI:10.1523/JNEUROSCI.0405-16.2016

Copyright © 2016 the authors 0270-6474/16/366213-12$15.00/0

lace et al., 2002; Scheffer et al., 2007). *SCN1B-C121W*, the first reported GEFS+ mutation, disrupts a critical, intramolecular disulfide bond within the extracellular β1 Ig loop domain (Wallace et al., 1998; Wallace et al., 2002; Audenaert et al., 2003; Barbieri et al., 2012). The impact of the *SCN1B-C121W* GEFS+ mutation on β1-subunit function is incompletely understood. Wild-type (WT) β1 subunits promote cellular aggregation *in vitro* via *trans*-homophilic cell–cell adhesion (Malhotra et al., 2000). In contrast, although mutant β1-C121W subunits are expressed at the cell surface in heterologous cells, they do not participate in *trans*-homophilic adhesion when tested in a cellular aggregation assay (Meadows et al., 2002). The effects of mutant β1-C121W subunit expression on VGSC function have been investigated extensively in heterologous systems, but results are cell-type and VGSC α-subunit specific (Moran and Conti, 2001; Meadows et al., 2002; Tammaro et al., 2002; Lucas et al., 2005; Aman et al., 2009; Egri et al., 2012; Baroni et al., 2013). *Ex vivo* studies of brain slices from the heterozygous *Scn1b*$^{+/W}$ GEFS+ knock-in mouse model showed temperature-sensitive changes in AP threshold and firing (Wimmer et al., 2010; Reid et al., 2014). In addition, *Scn1b*$^{+/W}$ mice showed differences in dendritic branching in subicular neurons that may be consistent with defects in β1-mediated cell–cell adhesion (Wimmer et al., 2010; Reid et al., 2014). Although multiple *in vitro* studies have demonstrated β1-C121W polypeptide expression at the surface of heterologous cells in which cDNA was overexpressed (Meadows et al., 2002; Tammaro et al., 2002; Patino et al., 2011), viral transduction of mouse neurons predicted that β1-C121W may be retained inside the cell and thus is nonfunctional (Wimmer et al., 2010). Studies of homozygous *Scn1b*$^{W/W}$ knock-in mice, which have a severe phenotype similar to the epileptic encephalopathy Dravet syndrome, showed differences in dendritic branching consistent with defects in β1-mediated cell–cell adhesion (Wimmer et al., 2010; Reid et al., 2014). β1-C121W subunits failed to localize at axon initial segments (AISs) of subicular neurons in these mice; however, whether the mutant β1 polypeptides were expressed at the neuronal cell surface was not addressed (Wimmer et al., 2015).

Here, we compared *Scn1b-C121W* knock-in GEFS+ mice (*Scn1b*$^{+/W}$) (Wimmer et al., 2010) with mice expressing the *Scn1b-null* allele (*Scn1b*$^{+/-}$) (Chen et al., 2004) to determine whether the β1-C121W GEFS+ mutation results in simple loss-of-function or if it conveys a deleterious gain-of-function. We report that the thermal seizure phenotype of *Scn1b*$^{+/W}$ GEFS+ mice is more severe than that of *Scn1b*$^{+/-}$ mice. β1-C121W polypeptides are expressed at the cell surface of cultured *Scn1b*$^{W/W}$ mouse neurons; however, they are expressed at lower levels than WT β1 polypeptides in *Scn1b*$^{+/+}$ brains. β1-C121W appears to be incompletely glycosylated compared with WT β1 polypeptides and its association with VGSC α subunits is disrupted. β1-C121W subunits localize to neuronal cell bodies in *Scn1b*$^{W/W}$ mouse brain cortex and cerebellum, but, unlike WT β1 subunits, are not translocated to specialized axonal subcellular domains, including the AIS and nodes of Ranvier. Together, our results suggest that the *Scn1b-C121W* GEFS+ mutation confers deleterious gain-of-function effects *in vivo*.

## Materials and Methods

*Mice.* *Scn1b*$^{+/-}$, *Scn1b*$^{-/-}$, *Scn1b*$^{+/W}$, and *Scn1b*$^{W/W}$ mice of both sexes were generated from *Scn1b*$^{+/-}$ and *Scn1b*$^{+/W}$ mice as described previously (Chen et al., 2004; Wimmer et al., 2010). *Scn1b*$^{+/-}$ mice were >N20 on the C57BL/6J background strain. *Scn1b*$^{+/W}$ mice were generated using C57BL/6J mouse embryonic stem cells and maintained on the C57BL/6J strain for >5 generations. Therefore, *Scn1b*$^{+/+}$ mice from *Scn1b*$^{+/W}$ × *Scn1b*$^{+/W}$ crossings are congenic C57BL/6J. Despite this, to be confident that there were no background differences, we compared *Scn1b*$^{+/+}$ mice from *Scn1b*$^{+/W}$ × *Scn1b*$^{+/W}$ litters and *Scn1b*$^{+/-}$ × *Scn1b*$^{+/-}$ litters in all experiments. No significant differences were observed between *Scn1b*$^{+/+}$ mice generated from either line. Animals were housed in the Unit for Laboratory Animal Medicine at the University of Michigan. All procedures were approved by the University of Michigan Institutional Animal Care and Use Committee.

*Thermal seizures.* Mice were tested for thermal seizure susceptibility at four developmental ages: postnatal day 15 (P15), P16, P20–P21, and P30–P33. Seizures were classified according to a modified Racine scale, as described previously (Racine, 1972; Patino et al., 2009). The scale used is as follows: 0 = no response; 1 = staring or unresponsive; 2 = focal or clonic convulsion involving twitches or myoclonic jerk of a single limb, head nods, or backing; 3 = clonus of both forelimbs; 4 = rearing/uncontrolled hind limbs without loss of posture; 5 = loss of upright posture usually preceded by jumping/rearing; and 6 = prolonged convulsion (≥30 s of tonic/clonic convulsions with loss of posture) or death. Due to the difficulty in observing level 1 seizures accurately without an EEG, seizures rated as level 1 were not recorded. Therefore, all seizures used in this analysis were of level 2 or greater. After a 1 ml intraperitoneal injection of 0.9% NaCl to prevent dehydration, a rectal thermometer was positioned to monitor body temperature (BT). A heat lamp connected to the monitor controlled BT according to the following protocol. Mice were acclimated with set temperature (ST) at 37°C for 30 min. Then, during the observation period, ST was increased by 0.5°C every 2 min. At the 20 min time point, ST was held at 42.5°C for an additional 15 min. When a seizure was observed, the following were recorded: BT, seizure severity (Racine scale), and time elapsed from the beginning of the observation period. After the experiment, all animals were killed and vital organs were removed. Genotypes were blinded to the observer and experiments were balanced as to sex of the animals. No significant differences were noted between female and male animals. WT animals from *Scn1b*$^{+/-}$ and *Scn1b*$^{+/W}$ litters were considered separate groups and compared directly during analysis. However, no significant differences were observed between WT genotypes, so these animals were pooled for final analysis. The numbers of mice used for the P15, P16, P20–P21, and P30–P33 age groups were as follows: *Scn1b*$^{+/+}$, $n = 22, 24, 20, 25$; *Scn1b*$^{+/-}$, $n = 16, 16, 18, 23$; and *Scn1b*$^{+/W}$, $n = 16, 11, 11, 17$, respectively.

*Behavioral seizure analysis.* For hyperthermia-induced seizure studies, temperature and time to first seizure were analyzed using the Mantel–Cox test. The most severe seizure for each mouse was analyzed using the Kruskal–Wallis test. Mann–Whitney analysis of these data gave similar results. For all analyses, $p \leq 0.05$ was the threshold for significance. *p*-values from all analyses are listed in Table 1.

*Antibodies.* Primary antibodies were as follows: rabbit anti-*Scn1b* (directed against an intracellular β1 epitope; Cell Signaling Technology, preproduction serum of D4Z2N, catalog #14684, 1:3000 used for Western blotting); rabbit anti-*Scn1b* (directed against an extracellular β1 epitope; Cell Signaling Technology, preproduction serum of D9T5B, catalog #13950, 1:25 used for immunofluorescence in optic nerves); rabbit anti-*Scn1b* (directed against an extracellular β1 epitope; Cell Signaling Technology, production version of D9T5B, catalog #13950, 1:250 used for immunofluorescence in brains); guinea pig anti-Caspr (gift from Dr. James Salzer, New York University School of Medicine, 1:1000 used for immunofluorescence in optic nerves); mouse anti-PAN VGSC α-subunit (Sigma-Aldrich, catalog #S8809, 1:200 used for immunofluorescence in optic nerves and co-immunoprecipitation); goat anti-ankyrinG (recognizing total ankyrinG, gift from Dr. Vann Bennett, He et al., 2014; Jenkins et al., 2015, 1:500 used for immunofluorescence in brains); mouse anti-calbindin (Sigma-Aldrich, catalog #C9848, 1:400 used for immunofluorescence in brains); rat anti-Ctip2 (Abcam, catalog #ab18465, 1:400 used for immunofluorescence in brains); rabbit anti-PAN VGSC α-subunit (Cell Signaling Technology, D2I9C, catalog #14380, 1:1000 used for Western blotting); mouse anti-human α-tubulin (Cedarlane Laboratories, catalog #CLT9002; 1:5000, used for Western blotting); mouse anti-HSP90 (Enzo Life Sciences, catalog #AC88, 1:1000, used for

**Table 1. Statistical values for thermal seizure experiments**

| | | | | | | *p*-values | | |
|---|---|---|---|---|---|---|---|---|
| | | WT | +/− | +/W | | WT vs +/− | WT vs +/W | +/W vs +/− |
| Time to first seizure (min) | | | | | | | | |
| P15 | Median | 20.6 | 20.91 | Mantel–Cox | 0.605 | <0.0001**** | <0.0001**** | |
| P16 | | 22.18 | 21.45 | | 21.37 | 0.5785 | 0.9288 | 0.583 |
| P15 vs P16 | *p*-value | 0.3877 | 0.4453 | | 0.0004*** | | | |
| P20–P21 | Median | Undefined | Undefined | | 26.05 | | 0.3818 | |
| P30–P33 | | Undefined | Undefined | | Undefined | | 0.3101 | |
| Temperature (°C) at first seizure | | | | | | | | |
| P15 | Median | 42.3 | >42.5 | 41.5 | Mantel–Cox | 0.7113 | 0.0022** | 0.0001*** |
| P16 | | 42.55 | 42.6 | 42.5 | | 0.199 | 0.6065 | 0.1677 |
| P15 vs P16 | *p*-value | 0.2643 | 0.7768 | 0.019* | | | | |
| P20–P21 | Median | >42.5 | >42.5 | >42.5 | | 0.5851 | | |
| P30–P33 | | >42.5 | >42.5 | >42.5 | | 0.4667 | | |
| Most severe seizure (*n*) | | | | | | | | |
| P15 | Mean ± SD | 3.45 ± 0.40 (22) | 4.313 ± 0.35 (16) | 5.250 ± 0.28 (16) | Kruskal–Wallis | ns | ** | ns |
| P16 | | 2.75 ± 0.42 (24) | 3.25 ± 0.42 (11) | 3.00 ± 0.77 (16) | | | ns | |
| P20–P21 | | 1.70 ± 0.53 (20) | 2.211 ± 0.60 (19) | 2.545 ± 0.77 (11) | | | ns | |
| P30–P33 | | 1.042 ± 0.34 (25) | 2.846 ± 0.78 (23) | 2.286 ± 0.69 (17) | | | ns | |

Temperature and time to first seizure comparisons were made using Mantel–Cox analysis and median is shown. The most severe seizure that each mouse experienced throughout the experiment is expressed as mean ± SD for the genotype and compared using Kruskal–Wallis analysis as described in the Materials and Methods. At P15, *Scn1b* $^{+/W}$ mice experienced their first seizure significantly sooner in the experiment and at a lower body temperature compared with *Scn1b* $^{+/+}$ and *Scn1b* $^{+/-}$ mice. P15 *Scn1b* $^{+/W}$ mice also experienced significantly more severe seizures compared with *Scn1b* $^{+/+}$ and *Scn1b* $^{+/-}$ mice. However, at P16, P20–P21, and P30–P33, there were no significant differences in seizure susceptibility between genotypes. All groups have >11 mice. See the Materials and Methods for descriptions of statistical analysis.

ns, Not significant. *, $p < 0.05$; **, $p < 0.01$; ***, $p < 0.001$; ****, $p < 0.0001$.

Western blotting). Secondary antibodies for Western blotting were as follows: HRP-conjugated goat anti-mouse (1:500; Thermo Fisher Scientific), HRP-conjugated goat anti-rabbit (1:500; Thermo Fisher Scientific). Secondary antibodies from Thermo Fisher Scientific, used for immunofluorescence at a 1:500 dilution, were as follows: Alexa Fluor goat anti-rabbit 488 nm, Alexa Fluor goat anti-mouse 594 nm, Alexa Fluor goat anti-guinea pig 647 nm, Alexa Fluor donkey anti-rabbit 488 nm, Alexa Fluor donkey anti-goat 594 nm, Alexa Fluor donkey anti-rat 594 nm, and Alexa Fluor donkey anti-mouse 647 nm.

*Mouse brain membrane preparation.* Mouse brain membrane proteins were prepared as described previously (Isom et al., 1995a). Complete protease inhibitors (Roche Diagnostics) were added to all solutions at twice the recommended concentration to minimize protein degradation. Briefly, immediately after anesthetization of the animal by isoflurane, brains were dissected and homogenized in ice-cold Tris-EGTA (50 mM Tris, 10 mM EGTA, pH 8.0). A polytron homogenizer was used to shear the tissue mechanically, followed by 20 strokes of homogenization in a chilled glass homogenizer. Homogenates were centrifuged at 2500 × *g* for 20 min at 4°C in a swinging bucket rotor to separate homogenized proteins from cell debris and nuclei. The supernatant was then ultracentrifuged (Thermo Fisher Scientific, Sorvall WX Ultra 80 ultracentrifuge) at 148,000 × *g* for 55 min at 4°C in a fixed-angle rotor (Thermo Fisher Scientific, TFT-80.4). The final pellet was resuspended in ice-cold Tris-EGTA and analyzed for protein concentration using the BCA assay (Thermo Fisher Scientific). Protein sample aliquots were stored at −80°C.

*Western blot analysis.* Western blots were performed as described previously (Malhotra et al., 2000). SDS sample buffer (final concentration, 62 mM Tris-HCl, 10% glycerol, 34 mM SDS, 20 mM dithiothreitol, 5% β-mercaptoethanol) was added to protein samples before separating by SDS-PAGE gels. Hand-poured 10%, 12%, 15%, and prepoured 4–15% (Bio-Rad) SDS-PAGE gels were used as indicated in the figure legends. With the exception of experiments using the mouse anti-HSP90 antibody, Western blots were performed using blocking solution containing 5% nonfat dry milk and 1% bovine serum albumin in TBST (0.1 M Tris-Cl, 0.5 M NaCl, pH 7.5, 0.1% Triton X-100), with primary antibodies incubated overnight at 4°C. For experiments using the anti-HSP90 antibody, a blocking solution of 2% nonfat dry milk in TBST was used and the primary antibody was incubated overnight at room temperature (RT). All secondary antibodies were applied for 1 h at RT. West Femto or West Dura reagent (Thermo Fisher Scientific, catalog #34095 or 34076) was used for detection. Immunoreactive signals were recorded using a Leica Odyssey Fc Imager.

*Coimmunoprecipitation.* For coimmunoprecipitation experiments, 200 μl of protein G-Sepharose beads (Sigma-Aldrich) were washed three times in PBS and divided equally into four microcentrifuge tubes. Beads were incubated overnight with end-over-end mixing at 4°C with 250 μl of dilution buffer (60 mM Tris/HCl, pH 7.5, 180 mM NaCl, 1.25% Triton X-100, 6 mM EDTA) and 5 μg of mouse anti-PAN VGSC antibody (Sigma-Aldrich) or 1.2 μg of mouse IgG (Jackson ImmunoResearch). Freshly thawed mouse brain membrane protein preparations (~1.2 mg of *Scn1b* $^{+/+}$ or *Scn1b* $^{W/W}$ for Fig. 4*A*; ~1.2 mg of *Scn1b* $^{+/+}$ or ~2.4 mg of *Scn1b* $^{W/W}$ for Fig. 4*B*) were resuspended in dilution buffer (with complete protease inhibitors at twice the recommended concentration) to a concentration of ~2.4 mg/ml. Protein samples were centrifuged at 5000 × *g* for 5 min. To remove proteins that associate nonspecifically with the Sepharose beads, protein supernatants were precleared by incubation with 50 μl of protein G-Sepharose beads (washed 3 times in PBS, but not incubated with antibody or IgG) for 1 h at 4°C with end-over-end mixing. The Sepharose beads were pelleted by centrifugation at 3000 × *g* for 3 min. Protein supernatant was removed and added to protein G-Sepharose beads previously incubated overnight with antibody or IgG. The protein and beads were incubated at 4°C for 4 h with end-over-end mixing. Beads were washed 3 times with ice-cold wash buffer (50 mM Tris/HCl, pH 7.5; 150 mM NaCl; 0.02% SDS; 5 mM EDTA; 2× complete protease inhibitors) with 0.1% Triton X-100, and then washed once with wash buffer without 0.1% Triton X-100. Next, 25 μl of Western blot sample buffer (see "Western blot analysis" section) was added to beads and heated for 10 min at 85°C to elute proteins from the beads.

*Quantification of β1-immunoreactive bands.* Quantification of β1 immunoreactive bands on Western blots was performed using ImageJ (version 1.49). Tissues from four animals from each genotype were tested in three replicate experiments. Values were normalized for protein loading using α-tubulin. Protein levels for each experiment were normalized to the mean for *Scn1b* $^{+/+}$. Final analysis was performed using two-way ANOVA.

*PNGaseF digestion.* PNGaseF digestion of *Scn1b* $^{+/+}$ and *Scn1b* $^{W/W}$ mouse brain membrane proteins was performed as recommended by the manufacturer (New England BioLabs) with the following changes: frozen brain membrane protein samples were thawed on ice and 100 μg of protein with 1× glycoprotein denaturing buffer (New England BioLabs)

in a total volume of 15.6 μl was heated for 10 min at 85°C. Then, 2.4 μl of G7 buffer (New England BioLabs), 2.4 μl of NP40 (New England BioLabs), and 3.6 μl of PNGaseF (or $ddH_2O$ for mock digestion) were added for a total volume of 24 μl. Reactions were incubated at 37°C for 2 h. Western sample buffer was added to each sample and samples were separated by SDS PAGE followed by Western blot. For Western blots, 100 μg of untreated brain membrane protein were loaded as "input" controls.

*Primary culture of cortical neurons.* P0–P1 mouse cortices were isolated and digested in unsupplemented Neurobasal medium (Invitrogen) with 0.25% trypsin for 15 min at 37°C. Cortices were then washed in HBSS (Invitrogen) and cells dispersed with fire polished Pasteur pipets. Cells were purified on a 35%/25%/20%/15% Optiprep (Axis-Shield) density gradient. The bottom 2 fractions were collected, washed, and diluted with Neurobasal medium supplemented with 0.5 mM L-glutamine (Invitrogen), 1% penicillin/streptomycin (Invitrogen), and 2% B-27 supplement (Invitrogen). Then, 200 μl of cells were plated on 15-mm-diameter poly-D-lysine-precoated coverslips (Neuvitro) at a density of 250,000 cells/coverslip. After 24 h in a 37°C humidified 5% $CO_2$ incubator, 2 ml of the above supplemented Neurobasal medium was added. Fifty percent of the medium was replaced every third day and cells were used on the 16$^{th}$ day *in vitro*.

*Surface biotinylation.* Surface biotinylation of primary cultured neurons was performed using the Cell Surface Protein Isolation kit (Thermo Fisher Scientific, catalog #89881) with adaptations to the manufacturer's suggested protocol as follows. All solutions were provided in the kit and reactions were performed on ice unless otherwise indicated. Briefly, primary neurons, cultured as described above, were plated on coverslips and cultured in six-well plates, with each well containing one coverslip. The culture medium was removed and cells were gently washed twice with ice-cold PBS. Then, 1.5 ml of 0.25 mg/ml Sulfo-NHS-SS-Biotin in ice-cold PBS was added to each well. Plates were rocked gently at 4°C for 30 min to ensure even coverage of the cells with the labeling solution. Next, 150 μl of quenching solution was added to each well and plates were rocked at RT for 5 min. Contents of each well were then scraped and transferred to 50 ml conical tubes. Each well was washed with 1 ml of TBS and wash was added to the corresponding tube of cells. Cells were pelleted at 1000 × *g* for 10 min in a swinging bucket rotor. The pellet was washed gently with 5 ml of TBS and then repelleted. From this point, complete protease inhibitors (Roche Diagnostics) were added to all solutions at twice the recommended concentration to minimize protein degradation. Cells were then resuspended in 25–50 μl of lysis buffer. Cell lysates were stored at −80°C. After four to five rounds of culture and biotinylation, cell lysates from the same genotypes were thawed on ice and pooled to achieve sufficient protein for detection. Pooled cell lysates were sonicated with a pulse sonicator at 20% power every 5 min on ice for 30 min. Cell lysates were centrifuged at 10,000 × *g* for 2 min to remove cellular debris. Twenty microliters of each supernatant was saved for "total cell lysate" sample analysis and used to determine protein concentration. For Figure 3, ~40 μg of protein was loaded in the total cell lysate lanes. The remaining supernatant (~450 μg of protein per sample) was added to 100 μl of washed NeutrAvidin agarose beads and rotated end-over-end overnight at 4°C. The following day, beads were washed 3× for 5 min at 4°C with 500 μl of ice-cold wash buffer. Beads were then rotated for 1 h at RT with 25 μl of sample buffer containing 50 mM DTT to ensure complete elution. The entire sample for each genotype was loaded and designated as "surface proteins" in Figure 3.

*Immunohistochemistry.* P15 littermates of the indicated genotypes were anesthetized using isofluorane. Mice were cardioperfused with ~10 ml of PBS followed by ~10 ml of 4% paraformaldehyde (PFA). Tissues were postfixed (brains overnight, optic nerves for 15 min) in 4% PFA. Tissues were then cryoprotected in 10% sucrose followed by 30% sucrose overnight, flash frozen in 2-methylbutane, and stored at −80°C. Optic nerves were embedded in O.C.T. (Tissue-Tek) before freezing. Longitudinal 10 μm optic nerve sections and 20 μm coronal brain sections were cut on a Leica cryostat and stored at −20°C until processing for immunohistochemistry.

For immunohistochemistry, sections were dried and postfixed for 10 min with 4% PFA, washed 3 times for 5 min each with 0.05 M phosphate buffer (PB), incubated in blocking buffer (10% goat or donkey serum as appropriate, 0.3% Triton X-100, 0.1M PB) for ≥2 h in a humidified chamber. Brain sections were incubated with 1% SDS in PB for 5 min before washing steps. Sections were then incubated with primary antibodies (diluted in blocking buffer) overnight in a humidified chamber and washed 3 times for 10 min with 0.1M PB. From this point, all steps were performed in the dark to minimize photobleaching of secondary antibodies. Sections were incubated with Alexa Fluor-conjugated secondary antibodies (diluted in blocking buffer) for 2 h, washed 3 times for 10 min in 0.1M PB, dried, and coverslips were mounted using ProLong Gold anti-fade reagent (Life Technologies). Finally, brain sections were incubated with DAPI for 20 min before mounting.

Sections were imaged using a Nikon A1R confocal microscope with Nikon NIS-Elements Advanced Research software located in the University of Michigan Department of Pharmacology using either a 60× numerical aperture (NA) 1.40 oil objective or a 20× NA 0.75 dry objective. Optic nerve sections were imaged using 3.1× digital zoom and Nyquist settings. All other settings were identical for all sections imaged in each experiment. For each optic nerve section, ≥3 single-section images were taken for analysis. Confocal images spanning 3 μm were acquired at 0.15 μm intervals and flattened using maximal signal for presentation in Figure 5. Images were analyzed as described below. Cortical and cerebellar confocal images spanning 10 μm were acquired at 0.175 μm intervals (for 60×) or 1.1 μm intervals (for 20×) and flattened using maximum signal for presentation in Figures 6 and 7.

*Quantification of β1 immunofluorescence.* For node of Ranvier studies, optic nerves from four to six animals per genotype were analyzed. Each animal was stained in at least three of four total independent immunohistochemistry experiments, with at least four optic nerve sections from each animal used in each experiment. Using NIS-Elements Advanced Research software (Nikon), the "region of interest" function was used to outline the area of each complete node in each image. In this step, only anti-PAN VGSC and anti-Caspr signals were made visible, thus blinding the observer to the anti-β1 signal. The software was then used to quantify the average anti-β1 and anti-PAN VGSC signal intensities for each region of interest. To remove nodes that were out of the plane of focus, nodes with the lowest 20% of anti-PAN VGSC signal were discarded before analysis. The average anti-β1 signal intensity per node for each optic nerve sample was used in final analysis (four optic nerves per animal per experiment). These values were normalized by setting the mean of all WT animals and the mean for all knock-out animals for the experiment to 1 and 0, respectively, using the "normalize" function in GraphPad Prism. Normalized values were analyzed using a linear mixed-model analysis performed using SPSS Statistics software (IBM) to account for variation between experiments and for variation between genotypes. The four comparisons indicated in Figure 5*B* were determined using this analysis and then correcting for multiple comparisons by multiplying each *p*-value by the number of comparisons.

For AIS experiments, three to four animals per genotype were used and two to three brain sections per animal per region were imaged for analysis. In all cases, sections obtained from the same locations relative to bregma were chosen. For cortex, imaging was done in the same region in both layer 2/3 and layer 5/6 of the somatosensory cortex, with one image per section per region for each animal. For cerebellum, three images per section for each animal were obtained from the same regions of the simple lobule of the cerebellum. Images were imported into ImageJ using the BioFormats plugin and flattened as described above. For each image, AISs were first identified as regions of linear ankyrinG immunolabeling and then evaluated for coincident linear β1 immunolabeling using the colocalization finder plugin for ImageJ, followed by visual reassessment of each identified AIS for confirmation. AISs positive for β1 were counted and results expressed as percentage of positive AISs per field of view. Due to unequal numbers of animals per genotype, statistical ANOVA was not appropriate. Therefore, the percentage of β1 positive AISs per field of view was analyzed using a linear mixed-model analysis performed using SPSS software (IBM). *p*-values were corrected for multiple comparisons by multiplying by the number of comparisons.

*Statistics.* All statistical analyses were performed using GraphPad Prism software unless otherwise indicated, with significance defined as $p < 0.05$.

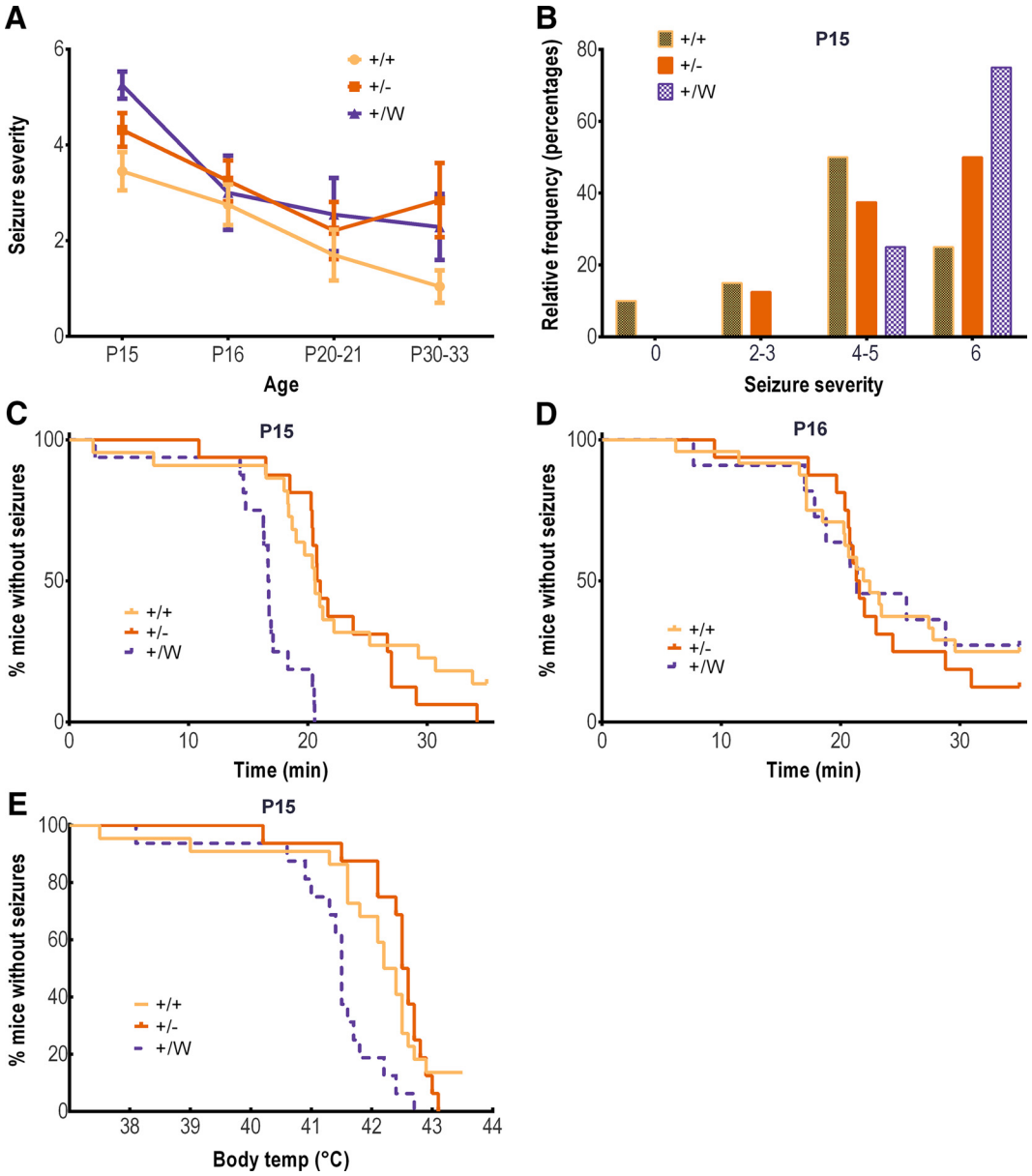


**Figure 1.** *Scn1b* $^{+/W}$ GEFS+ mice are more susceptible to heat-induced seizures than are *Scn1b* $^{+/-}$ and *Scn1b* $^{+/+}$ mice. Behavioral seizures were observed and Racine scores recorded by an investigator blinded to genotype. Seizures were induced as described in Materials and Methods. ***A***, Seizure severity recorded for each animal measured according to the modified Racine scale (mean ± SEM). Genotypes were compared at the same age. (Kruskal–Wallis, $p < 0.001$, *Scn1b* $^{+/W}$ vs *Scn1b* $^{+/+}$; $p < 0.05$ *Scn1b* $^{+/W}$ vs *Scn1b* $^{+/-}$). ***B***, Histogram of the most severe seizures at P15 showing that 75% of *Scn1b* $^{+/W}$ GEFS+ mice experienced a seizure of Racine score 6, compared with 25% or 50% of *Scn1b* $^{+/+}$ or *Scn1b* $^{+/-}$, respectively. ***C–E***, Survival curves to first observed seizure for P15 (***C***, ***E***) and P16 (***D***) mice in relation to time (***C***, ***D***) or BT (***E***). ***C***, At P15, *Scn1b* $^{+/W}$ GEFS+ mice experienced seizures sooner in the observation period than the other genotypes (Mantel–Cox, $p < 0.0001$, *Scn1b* $^{+/W}$ vs *Scn1b* $^{+/+}$; $p < 0.0001$, *Scn1b* $^{+/W}$ vs *Scn1b* $^{+/-}$ mice). ***D***, Difference shown in ***C*** was not observed at P16. ***E***, *Scn1b* $^{+/W}$ GEFS+ mice seized at lower BTs than *Scn1b* $^{+/+}$ or *Scn1b* $^{+/-}$ mice (Mantel–Cox; $p < 0.0001$, $p < 0.01$, respectively). Number of animals for the P15, P16, P20–P21, and P30–P33 groups were as follows: *Scn1b* $^{+/+}$, $n = 22$, 24, 20, 25; *Scn1b* $^{+/-}$, $n = 16$, 16, 18, 23; and *Scn1b* $^{+/W}$, $n = 6$, 11, 11, 17, respectively.

## Results

### *Scn1b* $^{+/W}$ GEFS+ mice are more susceptible to thermal seizures than *Scn1b* $^{+/-}$ mice

To determine whether the *SCN1B-C121W* GEFS+ mutation results in simple loss-of-function or whether it confers a deleterious gain-of-function *in vivo*, we compared mice expressing the *Scn1b*-null allele (Chen et al., 2004) with mice expressing the human *SCN1B-C121W* GEFS+ knock-in allele (Wimmer et al., 2010), both congenic on the C57BL/6 strain. Herein, the heterozygous and homozygous animals from these strains are indicated as *Scn1b* $^{+/-}$, *Scn1b* $^{-/-}$, *Scn1b* $^{+/W}$, and *Scn1b* $^{W/W}$, respectively. Previous work has shown that *Scn1b* $^{+/W}$ GEFS+ mice do not seize spontaneously (Wimmer et al., 2010). We have not observed spontaneous seizures in *Scn1b* $^{+/-}$ mice since their generation in 2004 (C. Chen and L.L.I., unpublished results and Chen et al., 2004). In addition, *Scn1b* $^{+/W}$ GEFS+ mice seize at lower BTs than their WT littermates in thermal seizure experiments (Wimmer et al., 2010). We compared the thermal seizure susceptibility of the two mouse lines at time points between P15 and P33 (P15, P16, P20–P21, and P30–P33) using a protocol described previously (Oakley et al., 2009). To evaluate potential genetic background effects between models, we tested WT littermates from both mouse lines for all thermal seizure, protein analysis, and immunostaining experiments presented herein. We

observed no significant differences between *Scn1b*$^{+/+}$ mice derived from *Scn1b*$^{+/-}$ × *Scn1b*$^{+/-}$ litters and *Scn1b*$^{+/+}$ mice derived from *Scn1b*$^{+/W}$ × *Scn1b*$^{+/W}$ litters. Therefore, for analyses presented here, results from these two WT groups were pooled, allowing a direct comparison of *Scn1b*$^{+/W}$ with *Scn1b*$^{+/-}$ mice. Overall, for both genotypes, younger mice had more severe seizures, seized at lower BTs, and had a shorter latency to first seizure compared with older mice of the same genotype (Fig. 1*A*, Table 1), suggesting that seizure susceptibility using this model is age dependent, similar to other models of pediatric seizures (Chung et al., 2013; Makinson et al., 2014).

We observed a significant difference in seizure phenotype between *Scn1b*$^{+/W}$ GEFS+ and *Scn1b*$^{+/-}$ mice at P15. At this time point, *Scn1b*$^{+/W}$ mice seized more severely than either WT or *Scn1b*$^{+/-}$ mice ($p = 0.0141$ and $p = 0.0443$, respectively; Fig. 1*A*,*B*). Seventy-five percent of *Scn1b*$^{+/W}$ GEFS+ mice experienced prolonged convulsions (with or without death) during the experimental period (recorded as Racine score 6) compared with 50% of *Scn1b*$^{+/-}$ mice and 25% of *Scn1b*$^{+/+}$ mice (Fig. 1*B*). Furthermore, latency to first seizure and BT at first seizure, as represented by time-to-event curves, were both significantly reduced in *Scn1b*$^{+/W}$ GEFS+ mice compared with *Scn1b*$^{+/-}$ mice ($p < 0.0001$ and $p < 0.01$, respectively; Fig. 1*C*,*E*). Together, these data indicate that *Scn1b*$^{+/W}$ GEFS+ mice, but not *Scn1b*$^{+/-}$ mice, are significantly more susceptible to heat-induced seizures than WT. In comparison, at P16 and at older ages (P20–P21 and P30–P33), there were no significant differences in any thermal seizure parameters among *Scn1b*$^{+/W}$, *Scn1b*$^{+/-}$, or *Scn1b*$^{+/+}$ mice (Fig. 1*A*,*D*, Table 1). As discussed above, it is unlikely that the observed differences between *Scn1b*$^{+/W}$ and *Scn1b*$^{+/-}$ mice were the result of residual genetic background differences between the mouse lines. The observation that *Scn1b*$^{+/W}$ GEFS+ and *Scn1b*$^{+/-}$ mice are different in terms of thermal seizure susceptibility is strong evidence that the human *SCN1B-C121W* GEFS+ mutation is not a simple loss-of-function allele and suggests instead that it confers a deleterious gain-of-function.

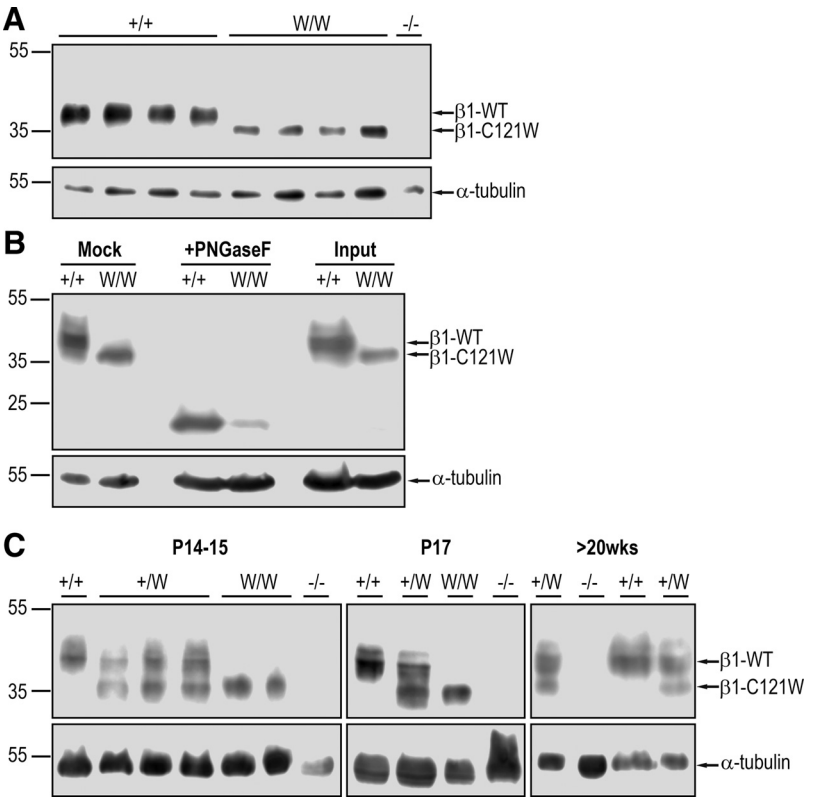


**Figure 2.** Comparison of β1-C121W and WT β1 protein expression. ***A***, Representative Western blots comparing anti-β1 immunoreactivity in *Scn1b*$^{+/+}$ and *Scn1b*$^{W/W}$ mouse brain membrane preparations. β1-C121W polypeptides migrate at a lower apparent molecular weight than WT β1 separated on a 10% SDS-PAGE gel. Immunoreactive bands were quantified using densitometry. Each band density was first normalized to its corresponding α-tubulin signal and β1 levels in *Scn1b*$^{W/W}$ mice were expressed as a percentage of β1 in *Scn1b*$^{+/+}$ mice. *Scn1b*$^{W/W}$ mice had 45 ± 10% of *Scn1b*$^{+/+}$ β1 expression (2-way ANOVA; $p = 0.0001$; 3 replicate experiments with 4 animals of each genotype). ***B***, Representative Western blots showing mock-digested, PNGaseF-digested, and control brain membrane inputs from *Scn1b*$^{+/+}$ and *Scn1b*$^{W/W}$ brains separated on a 12% SDS-PAGE gel. WT β1 and β1-C121W polypeptides migrate at similar molecular weights after removal of *N*-linked glycosylation by PNGaseF ($n = 3$). ***C***, Representative Western blots, separated on a 15% SDS-PAGE gel, comparing levels of WT β1 and β1-C121W polypeptides in P14–P15, P17, and >20-week-old *Scn1b*$^{+/+}$, *Scn1b*$^{+/W}$, and *Scn1b*$^{W/W}$ mice. α-tubulin is shown as a loading control. Every *Scn1b*$^{W/W}$ mouse tested showed the lower molecular band only (P14–P15, $n = 5$; P17, $n = 5$). Every *Scn1b*$^{+/W}$ sample tested showed both bands (P14–P15, $n = 11$; P17, $n = 6$; >20 weeks, $n = 4$).

### β1-C121W protein is expressed at lower levels in brain and may be incompletely glycosylated compared with WT

We next compared levels of WT β1 and β1-C121W polypeptide expression in brain membrane preparations from *Scn1b*$^{+/+}$ and *Scn1b*$^{W/W}$ mice, respectively. Separation of equivalent amounts of total protein on 10% SDS-PAGE gels followed by Western blotting with anti-β1 antibody showed that the level of β1-C121W expression in brain was ~50% of WT β1 (Fig. 2*A*). In addition, the β1-C121W-immunoreactive band migrated at a lower apparent molecular weight compared with WT β1 (Fig. 2*A*). This molecular weight difference was not observed in our previous heterologous expression studies (Meadows et al., 2002) and thus may be tissue or species specific. PNGaseF digestion of brain membrane preparations before SDS-PAGE analysis to remove *N*-linked glycosylation abrogated this apparent molecular weight difference (Fig. 2*B*), suggesting differences in posttranslational modification between WT β1 and β1-C121W proteins in brain *in vivo*. Finally, the absence of anti-β1-immunoreactive signal in the *Scn1b*$^{-/-}$ lane confirmed antibody specificity (Fig. 2*A*).

Because aberrant posttranslational modification can alter protein targeting for degradation (Ellgaard and Helenius, 2003), we tested brain membrane preparations from mice at different ages for the presence of the β1-C121W lower-molecular-weight band. SDS-PAGE analysis of β1 polypeptides from *Scn1b*$^{+/+}$, *Scn1b*$^{+/W}$, and *Scn1b*$^{W/W}$ mice showed evidence for β1-C121W expression in all mice tested, even at >20 weeks of age (Fig. 2*C*). Therefore, β1-C121W polypeptide expression is maintained throughout mouse brain development and does not appear to decrease with age.

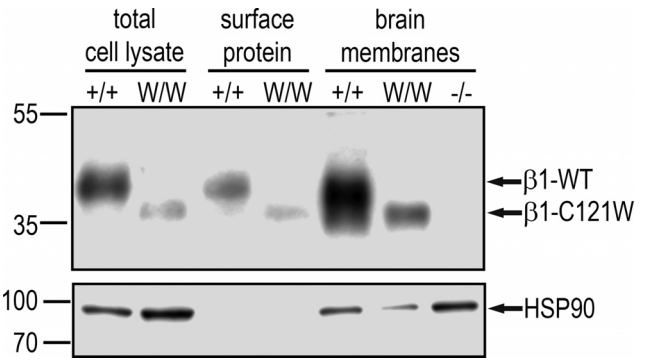


**Figure 3.** WT β1 and β1-C121W polypeptides are expressed at the neuronal cell surface in cultured mouse cortical neurons. Primary cortical neurons were cultured from *Scn1b* $^{+/+}$ and *Scn1b* $^{W/W}$ mice. At 16 DIV, surface proteins were labeled with biotin as described in the Materials and Methods. An aliquot of total cell lysate was reserved before performing immunoprecipitation with streptavidin beads to enrich for cell surface proteins. Total cell lysate for *Scn1b* $^{+/+}$ and *Scn1b* $^{W/W}$, along with control brain membrane samples, were separated on a 10% SDS-PAGE gel and immunoblotted with anti-β1 and anti-HSP90 antibodies. Anti-HSP90 immunoreactivity was used as an internal control to ensure enrichment of surface proteins in the biotinylated fraction. $n = 2$.

### β1-C121W polypeptides localize to the neuronal cell surface *in vivo*

Cell surface expression is required for VGSC subunit function. Although viral expression of a GFP-tagged β1-C121W construct in mouse neurons predicted intracellular retention (Wimmer et al., 2010), other studies of β1-C121W heterologous expression showed cell surface localization (Meadows et al., 2002; Patino et al., 2011). In addition, heterologous coexpression studies of β1-C121W and VGSC α subunits reported increased channel expression at the cell surface and/or increased sodium current compared with α subunits alone, predicting that β1-C121W localizes to the cell surface and retains the channel chaperone functions of β1 (Meadows et al., 2002; Tammaro et al., 2002; Rusconi et al., 2007; Baroni et al., 2013). To determine whether β1-C121W localizes to the cell surface of neurons *in vivo*, we performed surface biotinylation of cultured *Scn1b* $^{+/+}$ and *Scn1b* $^{W/W}$ cortical neurons. We detected WT β1 and β1-C121W polypeptides in both total cell lysate and biotinylated cell surface protein samples from *Scn1b* $^{+/+}$ and *Scn1b* $^{W/W}$ neurons, respectively (Fig. 3). As a control, the cytosolic protein HSP90 was detected in the cell lysate but not in the biotinylated samples, confirming the enrichment of cell surface proteins in the biotinylated fraction. These data suggest that endogenously expressed β1-C121W polypeptides are localized to the cell surface of cortical neurons *in vivo*.

### β1-C121W association with VGSC α-subunits is not detectable

A critical role for β1 subunits in brain is sodium current modulation via association with VGSC α-subunits (Chen et al., 2004; Brackenbury et al., 2010). Previous studies showed that overexpressed, recombinant β1-C121W protein could be coimmunoprecipitated with $Na_v1.1$, $Na_v1.2$, or $Na_v1.3$ α-subunits from solubilized, transfected cell lines (Meadows et al., 2002; Aman et al., 2009). However, these results may not reflect *in vivo* association of these subunits due to artifacts of heterologous overexpression. We therefore performed coimmunoprecipitation assays from mouse brain membrane preparations using anti-PAN-VGSC antibody followed by anti-β1 antibody to assess α-β1 association. We detected an α-WT β1, but not an α-β1-C121W, association in these samples,

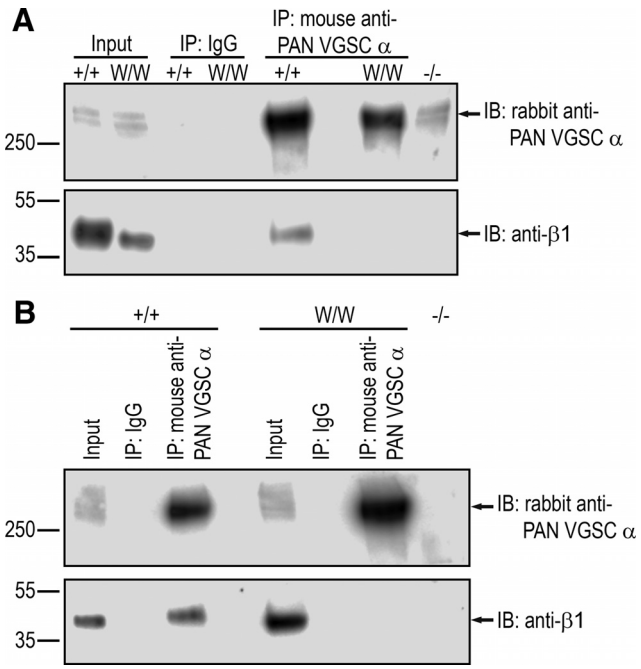


**Figure 4.** β1-C121W association with VGSC α-subunits is not detectable. Brain membrane proteins from P15 *Scn1b* $^{+/+}$ and *Scn1b* $^{W/W}$ animals were immunoprecipitated (IP) with either mouse IgG or mouse antibody against PAN VGSC α subunits. Input samples, IP samples for each genotype, and a control *Scn1b* $^{-/-}$ membrane sample were separated on a 4–15% SDS-PAGE gel and immunoblotted with rabbit anti-PAN VGSC and anti-β1 antibodies. ***A***, Representative Western blot of anti-PAN VGSC and anti-β1 coimmunoprecipitation using equivalent amounts of membrane proteins for each genotype. $n = 3$. ***B***, Western blot of anti-PAN VGSC and anti-β1 coimmunoprecipitation using twice as much *Scn1b* $^{W/W}$ as *Scn1b* $^{+/+}$ membrane protein to have equivalent amounts of β1 protein in the samples (see Fig. 2). Input samples were loaded in the same ratio to reflect the difference in starting protein. $n = 1$.

suggesting that β1-C121W does not associate with brain VGSC α subunits *in vivo* (Fig. 4*A*). Because the level of β1-C121W polypeptide expression is ~50% of the level of WT β1 in mouse brain (Fig. 2*A*), we repeated the coimmunoprecipitation experiment using twice the amount of *Scn1b* $^{W/W}$ starting material. Despite this increase, we did not detect β1-C121W and VGSC α-subunit association by coimmunoprecipitation (Fig. 4*B*). Therefore, whereas the *Scn1b*-C121W mutation does not affect β1 cell surface expression *in vivo*, it does appear to weaken or disrupt the VGSC α-β1 association.

### β1-C121W polypeptides localize differentially to neuronal subcellular domains

VGSC β1 subunits colocalize with VGSC α subunits at the AIS and nodes of Ranvier *in vivo* (Chen et al., 2004; Brackenbury et al., 2010; Wimmer et al., 2010; Wimmer et al., 2015). β1-mediated cell adhesive interactions may be particularly important at the nodes of Ranvier because *Scn1b-null* mice exhibit dysmyelination, reduced numbers of nodes, and disruption of axo-glial cell–cell contact in a subset of neurons (Chen et al., 2004). Therefore, we investigated whether β1-C121W is localized to these axonal subcellular domains *in vivo*.

We performed fluorescence immunohistochemistry of longitudinally sectioned WT and mutant mouse optic nerve and found that the level of β1 immunofluorescence was significantly decreased at nodes of Ranvier in *Scn1b* $^{W/W}$ mice compared with WT and similar to that observed in *Scn1b* $^{-/-}$ mice (Fig. 5*A*,*B*). Quantification of anti-β1 optic nerve nodal immunofluorescence signal across genotypes showed that *Scn1b* $^{+/W}$ levels were lower than *Scn1b* $^{+/+}$ but higher than *Scn1b* $^{+/-}$ (Fig. 5*B*).

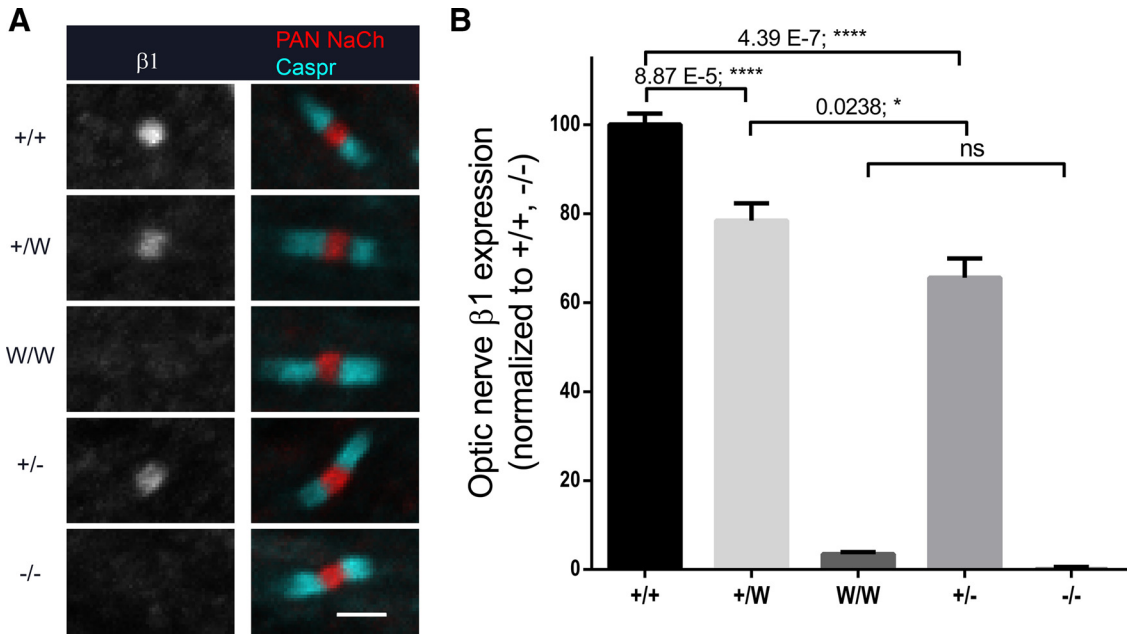


**Figure 5.** β1-C121W is not expressed at optic nerve nodes of Ranvier. ***A***, Representative images showing that *Scn1b*$^{+/W}$ and *Scn1b*$^{+/-}$ mice have decreased anti-β1 immunofluorescence compared with WT. Anti-β1 immunofluorescence in *Scn1b*$^{W/W}$ optic nerve sections is not significantly different from *Scn1b*$^{-/-}$. ***B***, Quantification, as described in Materials and Methods, of anti-β1 immunofluorescence at optic nerve nodes of Ranvier. Data represent four independent immunohistochemistry experiments, with four to six animals per genotype in total. Each animal was tested in at least three experiments. Linear mixed-model analysis was used to make comparisons between genotypes; see the Materials and Methods for further details. Scale bar, 2 μm.

We next examined WT β1 and β1-C121W immunofluorescence localization to the AIS in multiple brain regions. Anti-β1 immunofluorescence staining revealed a high percentage of β1-positive AIS domains in cortical layer II and VI neurons and in cerebellar Purkinje neurons in *Scn1b*$^{+/+}$, *Scn1b*$^{+/-}$, and *Scn1b*$^{+/W}$ mice (Fig. 6*A–C*, *J–L*, *D–F*, respectively). The anti-β1 antiserum used for these experiments was directed against an extracellular β1 epitope and specifically detected both WT β1 and β1-C121W polypeptides on Western blots (Fig. 6*Q*). In Figure 6, the left micrograph in the panel for each cortical region is a merged image showing staining for the AIS marker ankyrinG (red, arrows in Fig. 6*A*,*B*), β1 (green), and DAPI (blue); the center micrograph shows anti-β1 staining alone (white); and the right micrograph shows side-by-side magnified images of a single AIS showing merged anti-ankyrinG/β1/DAPI and anti-β1 staining, respectively. In panels showing cerebella, anti-calbindin staining (magenta) was used as a marker of Purkinje neurons, with the leftmost micrograph showing merged anti-ankyrinG (red, arrows in Fig. 6*C*,*F*)/anti-β1 (green)/anti-calbindin (magenta)/DAPI (blue) staining, followed by anti-β1 staining alone (white) and side-by-side zoomed images of a single AIS showing merged anti-ankyrinG/anti-β1/anti-calbindin/DAPI and anti-β1 staining, respectively. In *Scn1b*$^{W/W}$ cortical and Purkinje neurons, anti-β1 staining was observed at the soma (arrowheads), but not at the AIS (Fig. 6*G–I*). Both somal (arrowhead) and AIS (arrow) anti-β1 staining were observed in *Scn1b*$^{+/W}$ sections (Fig. 6*D–F*). These results suggest that mutant β1-C121W subunits do not prevent the translocation of WT β1 subunits to the axon. Anti-β1 staining was absent in *Scn1b*$^{-/-}$ brain sections, as expected, demonstrating antibody specificity (Fig. 6*M–O*). Quantification showed an absence of β1-positive AISs in layer II, VI, and cerebellar *Scn1b*$^{W/W}$ sections compared with *Scn1b*$^{+/+}$ and *Scn1b*$^{+/W}$ mice (Fig. 6*P*). There was a slight, but statistically significant, reduction in β1-positive AISs in layer II and VI *Scn1b*$^{+/W}$ sections compared with *Scn1b*$^{+/+}$ and *Scn1b*$^{+/-}$, although the biological significance of this observation is not clear. Staining of cortical brain sections with a different anti-β1 antibody (Oyama et al., 2006; used in Wimmer et al., 2015) also showed β1-positive AISs in *Scn1b*$^{+/+}$ neurons in layers II and VI, similar to those in Figure 6, *A* and *B* (data not shown). However, the large amount of nonspecific nuclear staining observed with this antibody precluded detection of cell body staining in *Scn1b*$^{+/W}$ and *Scn1b*$^{W/W}$ mice (data not shown) and explains why this was not reported previously (Wimmer et al., 2015). Anti-β1 staining observed in neuronal cell bodies in *Scn1b*$^{W/W}$ cortical neurons was layer specific. Figure 6, *G–I*, shows limited cell body staining in layers II and VI. In contrast, a much higher proportion of β1-positive cell bodies were identified as Ctip2-positive neurons in layer V (Fig. 7*B*,*C*,*G*,*H*), suggesting that β1-C121W localization may be neuronal-cell-type specific.

Together, our immunofluorescence and cell surface biotinylation results suggest that β1-C121W reaches the neuronal cell surface *in vivo*, but is not translocated to axonal subcellular domains and instead remains localized to neuronal soma.

## Discussion

The objective of this study was to determine the mechanism of how the *SCN1B-C121W* GEFS+ mutation alters VGSC β1 function *in vivo*. To address this question, we used a multidisciplinary approach that included behavioral, biochemical, and immunofluorescence analyses of transgenic mouse models. We report that *Scn1b*$^{+/W}$ GEFS+ mice are more susceptible to thermally induced seizures than *Scn1b*$^{+/-}$ or *Scn1b*$^{+/+}$ mice. Biochemically, β1-C121W polypeptides are expressed at lower levels than WT β1 in the brain and migrate at a lower apparent molecular weight by SDS-PAGE gels. PNGase digestion followed by Western blot analysis shows that this molecular weight difference is likely due to incomplete glycosylation of the mutant β1 polypeptide *in vivo*. Surface biotinylation assays showed that β1-C121W

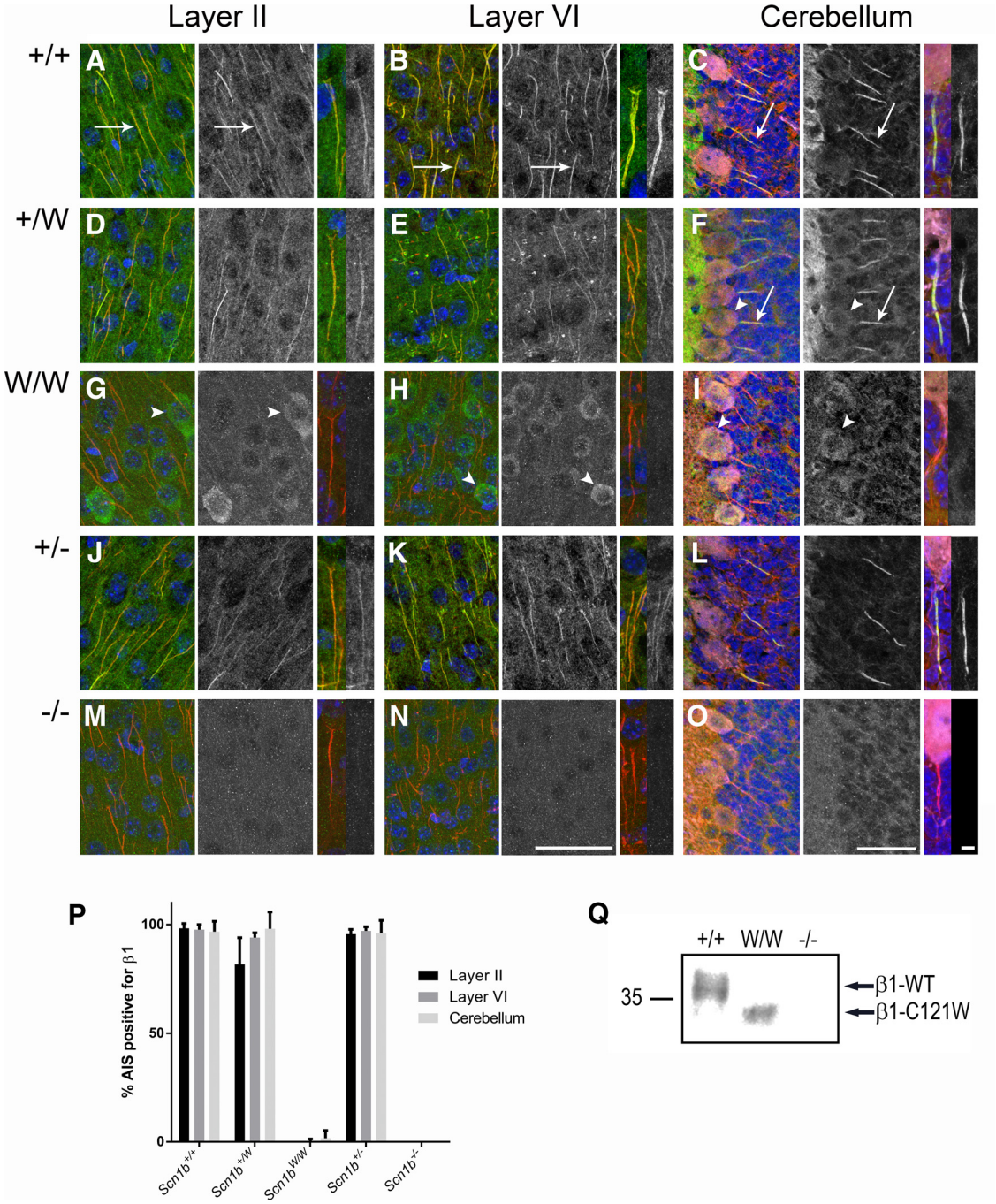


**Figure 6.** β1-C121W is not expressed at cerebellar or cortical axon initial segments. Representative confocal images of cortical layers II (***A***, ***D***, ***G***, ***J***, ***M***) and VI (***B***, ***E***, ***H***, ***K***, ***N***) and Purkinje cells in the cerebellum (***C***, ***F***, ***I***, ***L***, ***O***) of *Scn1b* $^{+/+}$ (***A–C***), *Scn1b* $^{+/W}$ (***D–F***), *Scn1b* $^{W/W}$ (***G–I***), *Scn1b* $^{+/-}$ (***J–L***), and *Scn1b* $^{-/-}$ (***M–O***) mice. For each genotype and cortical region, the left panel is a merged image of anti-ankyrinG (red), DAPI (blue), and anti-β1 (green) staining; the middle panel is anti-β1 (white) staining; and the right panel is a higher-magnification image of a single AIS with the merged image on the left and anti-β1 staining alone on the right. For cerebellum, merged images show anti-ankyrinG (red)/anti-β1 (green)/anti-calbindin (magenta)/DAPI (blue) staining. Arrows (***A–C***, ***F***) indicate examples of ankyrinG-positive, β1-positive AISs. Arrowheads (***F–I***) indicate examples of β1-positive soma in *Scn1b* $^{+/W}$ and *Scn1b* $^{W/W}$ mice. *Scn1b* $^{W/W}$ and *Scn1b* $^{-/-}$ mice showed no anti-β1 immunofluorescence at the AIS. Scale bars: large, 50 μm; small,10 μm. Three mice of each genotype were tested. ***P***, Quantification of AISs positive for anti-β1 immunofluorescence. For all regions observed, *Scn1b* $^{W/W}$ mice were comparable to *Scn1b* $^{-/-}$ mice and had a >95% reduction in β1-positive AISs compared with *Scn1b* $^{+/+}$ mice ($p < 0.0001$). In layers II and VI, *Scn1b* $^{+/W}$ mice had slightly fewer β1-positive AISs compared with *Scn1b* $^{+/+}$ and *Scn1b* $^{+/-}$ mice (layer II: 16.6 ± 2.0%, $p < 0.0001$, 14.0 ± 2.3%, $p < 0.0001$; layer VI: 3.7 ± 0.8%, $p < 0.0001$, 3.1 ± 0.9%, $p = 0.007$, respectively). ***Q***, Western blot showing anti-β1 immunoreactivity in brain membranes from *Scn1b* $^{+/+}$, *Scn1b* $^{W/W}$, and *Scn1b* $^{-/-}$ mice using the D9T5B anti-β1 antibody used for immunofluorescence in Figures 6 and 7.

polypeptides are expressed at the cell surface of cultured *Scn1b* $^{W/W}$ cortical neurons.

Immunofluorescence confocal microscopy demonstrated that β1-C121W localizes to the neuronal cell body in *Scn1b* $^{W/W}$ brain sections; however, the subcellular localization of these mutant β1 subunits is limited to the soma and precluded from the axon. Our available model and tools did not allow us to distinguish between WT and mutant β1 subunits by immunofluorescence in *Scn1b* $^{+/W}$ mice and thus to determine whether mutant β1 subunits also translocate to the axon in the presence of WT

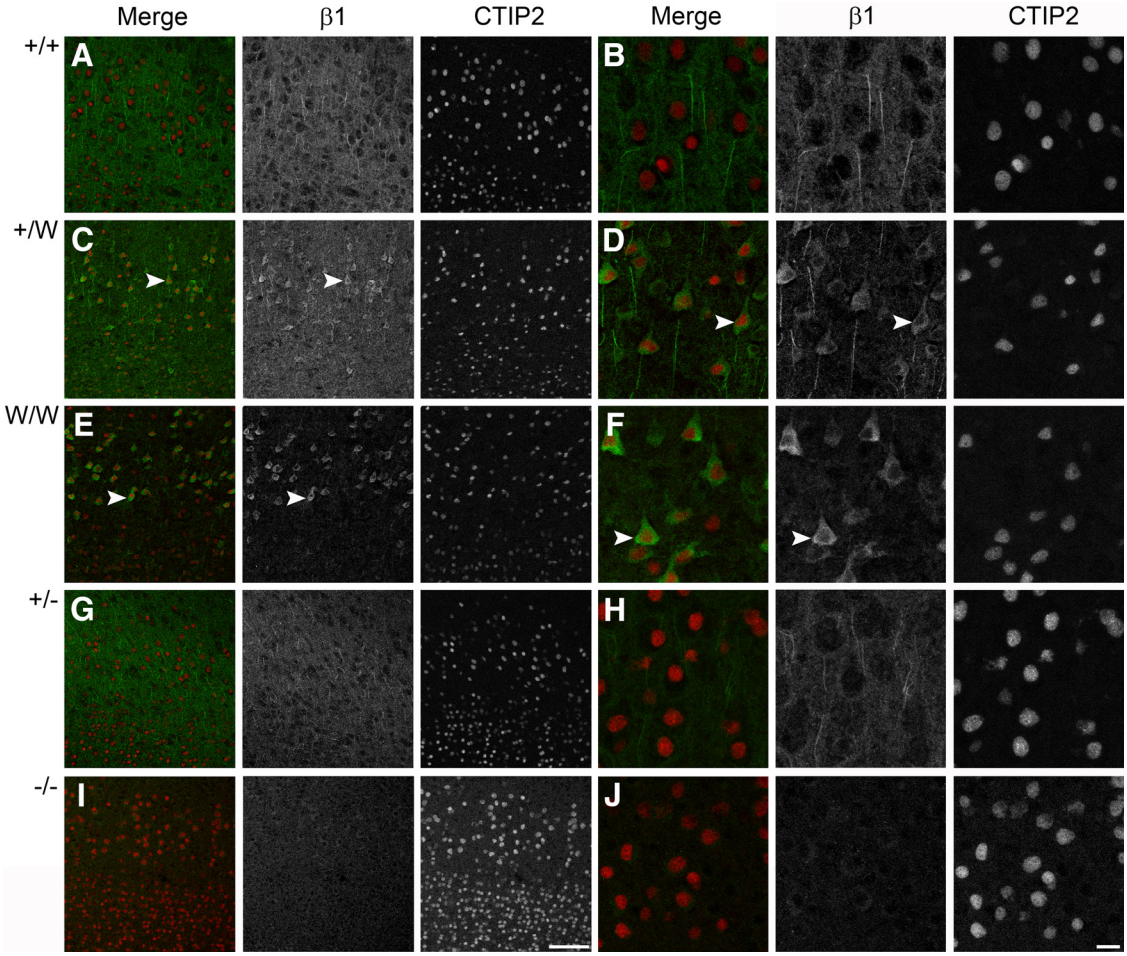


**Figure 7.** $\beta$1-C121W is localized at the soma of layer V cortical neurons. Representative confocal images of cortical layer V from *Scn1b* $^{+/+}$ (***A***, ***B***), *Scn1b* $^{+/W}$ (***C***, ***D***), *Scn1b* $^{W/W}$ (***E***, ***F***), *Scn1b* $^{+/-}$ (***G***, ***H***), and *Scn1b* $^{-/-}$ (***I***, ***J***) mice. The left panel for each genotype is a merged image of anti-Ctip2 (red) and anti-$\beta$1 (green) staining and the following two panels show anti-$\beta$1 (white) followed by anti-Ctip2 (white) staining. Arrowheads indicate examples of anti-$\beta$1-positive soma in *Scn1b* $^{+/W}$ and *Scn1b* $^{W/W}$ mice. Lower-magnification images (***A***, ***C***, ***E***, ***G***, ***I***) show the layer specificity of $\beta$1-positive soma. Higher-magnification images (***B***, ***D***, ***F***, ***H***, ***J***) showing Ctip2-positive layer V neurons are also presented. Scale bars: ***A***, ***C***, ***E***, ***G***, ***I***, 100 $\mu$m; ***B***, ***D***, ***F***, ***H***, ***J***, 20 $\mu$m. Three mice of each genotype were tested.

subunits. The observation that the level of anti-$\beta$1 immunofluorescence at optic nerve nodes of Ranvier is higher in *Scn1b* $^{+/W}$ GEFS+ compared with *Scn1b* $^{+/-}$ mice may suggest that WT and mutant $\beta$1 subunits may be present together in axonal domains. Alternatively, however, the observation of a small but significant reduction in $\beta$1-positive AISs in layer II and VI *Scn1b* $^{+/W}$ sections compared with *Scn1b* $^{+/+}$ and *Scn1b* $^{+/-}$ may suggest that mutant $\beta$1 subunits may prevent a portion of WT $\beta$1 subunits from entering the axon. Finally, even though $\beta$1-C121W is expressed at the cell surface in *Scn1b* $^{W/W}$ neurons, its association with VGSC $\alpha$ subunits is disrupted, as assessed by coimmunoprecipitation.

The crystal structure of the VGSC $\beta$1 Ig loop has not yet been solved. However, important information can be gleaned from the crystal structure of a VGSC $\beta$4 Ig loop containing a C to W mutation at residue 131, corresponding to $\beta$1-C121W (Gilchrist et al., 2013). Importantly, introducing this mutation in the disulfide cysteine bridge of $\beta$4, which is conserved in all five VGSC $\beta$ subunits, did not disrupt protein folding or plasma membrane trafficking compared with $\beta$4-WT, as assessed in *Xenopus* oocytes. However, the C to W mutation did disrupt the ability of $\beta$4 to modulate sodium current expressed by $Na_v1.2$ and resulted in potential alterations in $\beta$4 glycosylation (Gilchrist et al., 2013), similar to our present results for $\beta$1-C121W.

Our results, together with our previous data showing that $\beta$1-C121W cannot participate in *trans*-homophilic cell–cell adhesion (Meadows et al., 2002), suggest that the *SCN1B-C121W* GEFS+ mutation confers a deleterious gain-of-function. We propose that, in *Scn1b* $^{+/W}$ GEFS+ mice, nonfunctional $\beta$1-C121W subunits are expressed together with WT $\beta$1 subunits at the plasma membrane and thus effectively reduce the level of $\beta$1 function in neurons by diluting the density of WT subunits. $\beta$1-mediated *trans*-homophilic cell–cell adhesion may be particularly disrupted by this mechanism because WT–mutant or mutant–mutant $\beta$1 subunit pairs may be aligned, but not associate, in *trans* on adjacent axons, resulting in areas of aberrant adhesion and fasciculation. In addition, we propose that mutant $\beta$1B subunits, which are normally soluble ligands for cell adhesion (Patino et al., 2011), are co-secreted with WT $\beta$1B subunits in *Scn1b* $^{+/W}$ developing brains, yet are nonfunctional and effectively change the functionality of secreted WT $\beta$1B subunits. This scenario is different from in *Scn1b* $^{+/-}$ neurons, in which only the WT $\beta$1 and $\beta$1B subunits are expressed. In *Scn1b* $^{W/W}$ mice, which have a severe, epileptic encephalopathy-like phenotype and a pharmacosensitivity profile similar to patients with Dravet syndrome (Reid et al., 2014), all expressed $\beta$1 subunits are mutant and thus fail to associate with VGSC $\alpha$ subunits, fail to participate in cell–cell adhesion, and fail to translocate from the cell

body to axonal subcellular domains. Therefore, we propose that, whereas mutant β1 subunits are expressed at the neuronal cell surface in *Scn1b*$^{W/W}$ mice, this model is functionally similar to *Scn1b*-null mice, which have been shown to model Dravet syndrome (Patino et al., 2009).

In our previous work, we showed that covalent VGSC α-β2 association, via formation of an extracellular disulfide bond, is required for β2, but not α, subunit translocation to nodes of Ranvier (Chen et al., 2012). Our present results suggest that association with VGSC α subunits, although noncovalent (Hartshorne and Catterall, 1981), may be required for β1 translocation to axonal domains. We were unable to detect association between β1-C121W and VGSC α subunits and did not detect β1-C121W at the AIS or nodes of Ranvier in *Scn1b*$^{W/W}$ mice. Therefore, in a mechanism similar to α-β2 association, α-β1 association through extracellular domains may be required for proper β-subunit subcellular localization in neurons.

We proposed previously that β1 and β4 have opposing actions on neuronal excitability, with β4 acting as an "accelerator" and β1 acting as a "brake" via promotion of VGSC inactivation (Aman et al., 2009). Furthermore, we showed that β1-C121W did not exert the same modulatory effects on excitability as WT β1 (Aman et al., 2009). Previous electrophysiological analysis of brain slices from *Scn1b*$^{+/W}$ mice showed temperature-sensitive enhancement of AIS function leading to subicular pyramidal neuron hyperexcitability (Wimmer et al., 2010). Computational modeling of these data predicted that this increased excitability was caused by a hyperpolarizing shift in the voltage dependence of activation of pyramidal neuron AIS VGSCs. The investigators proposed that this contributed to heightened thermal seizure susceptibility in *Scn1b*$^{+/W}$ mice. Similar electrophysiological experiments performed in *Scn1b*$^{W/W}$ mice showed cortical layer 2/3 and subicular pyramidal neuron hyperexcitability with increased synaptic activity in the subiculum (Reid et al., 2014). Hyperexcitability was not observed in CA1 or cortical layer 5 pyramidal neurons or in hippocampal interneurons of *Scn1b*$^{W/W}$ mice, suggesting that the *in vivo* effects of *Scn1b* mutations are brain-region and neuronal-cell-type specific and, interestingly, that *Scn1b*-linked epileptic encephalopathy is not an interneuronopathy, as has been proposed for *Scn1a*-linked Dravet syndrome (Yu et al., 2006; Reid et al., 2014). Together with the present results, we propose that the inability of mutant β1-C121W subunits to associate with and modulate VGSC α subunits at the neuronal cell surface contributes to hyperexcitability in *SCN1B-C121W*-linked epilepsies.

In addition to modulating VGSCs, β1 subunits are known to associate with and stabilize voltage-gated potassium channels that express A-type current in neurons (Marionneau et al., 2012). Administration of the potassium channel opener retigabine to *Scn1b*$^{W/W}$ brain slices reversed the hyperexcitable phenotype and reduced thermal seizure susceptibility in *Scn1b*$^{W/W}$ mice (Reid et al., 2014). An important future experiment will be to assess the effect of the *SCN1B-C121W* mutation on β1 association with $K_v$4.2 in *Scn1b*$^{W/W}$ brains. Although we attempted these experiments, the solubilization conditions for immunoprecipitation of VGSCs and $K_v$4.2 channels using available antibodies were incompatible. Therefore, we were unable to determine whether β1-C121W subunits maintain their association with $K_v$4.2. In the future, with the availability of higher-quality antibodies, we may be able to assess whether aberrant β1-Kv association also contributes to the GEFS+ phenotype.

*SCN1B* mutations exhibit incomplete penetrance in human patients. *SCN1B-C121W*-linked GEFS+ has been shown to result in diverse clinical phenotypes from mild to complex, even within the same family (Scheffer et al., 2007; Helbig, 2015). The parents of a Dravet syndrome patient homozygous for the loss-of-function mutation *SCN1B-R125C*, who are each heterozygous for the mutation, did not report seizures (Patino et al., 2009). Furthermore, the Exome Aggregation Consortium (ExAC, http://exac.broadinstitute.org/) database reports several neurologically normal patients with predicted heterozygous loss-of-function *SCN1B* mutations, suggesting that *SCN1B* haploinsufficiency may be tolerated.

Together, our studies provide evidence for a complex molecular mechanism leading to changes in excitability and thermal seizure susceptibility in *Scn1b*$^{+/W}$ GEFS+ mice compared with *Scn1b*$^{+/-}$ mice. Unlike other epilepsy-associated *SCN1B* mutations (Patino et al., 2009), *SCN1B-C121W* does not appear to cause β1-subunit intracellular retention, but rather confers deleterious gain-of-function. Therefore, the mechanisms underlying *SCN1B*-linked epilepsy may be diverse, requiring the generation of animal models expressing specific patient mutations to better understand β1 and β1B physiology and pathophysiology. To date, nine unique *SCN1B* mutations in epilepsy patients have been reported (O'Malley and Isom, 2015). Using transgenic mouse and human patient-derived induced pluripotent stem cell models with strategies similar to the present study, a better understanding of the affected molecular pathways may lead to the development of novel therapeutics for patients with *SCN1B*-linked epilepsy. Moreover, because *SCN1B* epilepsy mutations are largely inherited, rather than *de novo*, effective genetic counseling strategies can be developed.

## References


Aman TK, Grieco-Calub TM, Chen C, Rusconi R, Slat EA, Isom LL, Raman IM (2009) Regulation of persistent Na current by interactions between beta subunits of voltage-gated Na channels. J Neurosci 29:2027–2042. CrossRef Medline

Audenaert D, Claes L, Ceulemans B, Löfgren A, Van Broeckhoven C, De Jonghe P (2003) A deletion in SCN1B is associated with febrile seizures and early-onset absence epilepsy. Neurology 61:854–856. CrossRef Medline

Barbieri R, Baroni D, Moran O (2012) Identification of an intra-molecular disulfide bond in the sodium channel beta1-subunit. Biochem Biophys Res Commun 420:364–367. CrossRef Medline

Baroni D, Barbieri R, Picco C, Moran O (2013) Functional modulation of voltage-dependent sodium channel expression by wild type and mutated C121W-beta1 subunit. J Bioenerg Biomembr 45:353–368. CrossRef Medline

Brackenbury WJ, Isom LL (2008) Voltage-gated Na+ channels: potential for beta subunits as therapeutic targets. Expert Opin Ther Targets 12:1191–1203. CrossRef Medline

Brackenbury WJ, Isom LL (2011) Na channel beta subunits: overachievers of the ion channel family. Front Pharmacol 2:53. CrossRef Medline

Brackenbury WJ, Calhoun JD, Chen C, Miyazaki H, Nukina N, Oyama F, Ranscht B, Isom LL (2010) Functional reciprocity between Na+ channel Nav1.6 and beta1 subunits in the coordinated regulation of excitability and neurite outgrowth. Proc Natl Acad Sci U S A 107:2283–2288. CrossRef Medline

Chen C, Westenbroek RE, Xu X, Edwards CA, Sorenson DR, Chen Y, McEwen DP, O'Malley HA, Bharucha V, Meadows LS, Knudsen GA, Vilaythong A, Noebels JL, Saunders TL, Scheuer T, Shrager P, Catterall WA, Isom LL (2004) Mice lacking sodium channel beta1 subunits display defects in neuronal excitability, sodium channel expression, and nodal architecture. J Neurosci 24:4030–4042. CrossRef Medline

Chen C, Calhoun JD, Zhang Y, Lopez-Santiago L, Zhou N, Davis TH, Salzer JL, Isom LL (2012) Identification of the cysteine residue responsible for

disulfide linkage of Na+ channel alpha and beta2 subunits. J Biol Chem 287:39061–39069. CrossRef Medline

Chung JI, Kim AY, Lee SH, Baik EJ (2013) Seizure susceptibility in immature brain due to lack of COX-2-induced PGF2alpha. Exp Neurol 249: 95–103. CrossRef Medline

Davis TH, Chen C, Isom LL (2004) Sodium channel $\beta$1 subunits promote neurite outgrowth in cerebellar granule neurons. J Biol Chem 279:51424–51432. CrossRef Medline

Egri C, Vilin YY, Ruben PC (2012) A thermoprotective role of the sodium channel beta1 subunit is lost with the beta1 (C121W) mutation. Epilepsia 53:494–505. CrossRef Medline

Ellgaard L, Helenius A (2003) Quality control in the endoplasmic reticulum. Nat Rev Mol Cell Biol 4:181–191. CrossRef Medline

Gilchrist J, Das S, Van Petegem F, Bosmans F (2013) Crystallographic insights into sodium-channel modulation by the beta4 subunit. Proc Natl Acad Sci U S A 110:E5016–E5024. CrossRef Medline

Hartshorne RP, Catterall WA (1981) Purification of the saxitoxin receptor of the sodium channel from rat brain. Proc Natl Acad Sci U S A 78:4620–4624. CrossRef Medline

He M, Abdi KM, Bennett V (2014) Ankyrin-G palmitoylation and betaII-spectrin binding to phosphoinositide lipids drive lateral membrane assembly. J Cell Biol 206:273–288. CrossRef Medline

Helbig I (2015) Genetic causes of generalized epilepsies. Semin Neurol 35: 288–292. CrossRef Medline

Isom LL, De Jongh KS, Patton DE, Reber BF, Offord J, Charbonneau H, Walsh K, Goldin AL, Catterall WA (1992) Primary structure and functional expression of the $\beta$1 subunit of the rat brain sodium channel. Science 256:839–842. CrossRef Medline

Isom LL, Scheuer T, Brownstein AB, Ragsdale DS, Murphy BJ, Catterall WA (1995a) Functional co-expression of the $\beta$1 and type IIA $\alpha$ subunits of sodium channels in a mammalian cell line. J Biol Chem 270:3306–3312. CrossRef Medline

Isom LL, Ragsdale DS, De Jongh KS, Westenbroek RE, Reber BF, Scheuer T, Catterall WA (1995b) Structure and function of the $\beta$2 subunit of brain sodium channels, a transmembrane glycoprotein with a CAM motif. Cell 83:433–442. CrossRef Medline

Jenkins PM, Kim N, Jones SL, Tseng WC, Svitkina TM, Yin HH, Bennett V (2015) Giant ankyrin-G: a critical innovation in vertebrate evolution of fast and integrated neuronal signaling. Proc Natl Acad Sci U S A 112: 957–964. CrossRef Medline

Lucas PT, Meadows LS, Nicholls J, Ragsdale DS (2005) An epilepsy mutation in the beta1 subunit of the voltage-gated sodium channel results in reduced channel sensitivity to phenytoin. Epilepsy Res 64:77–84. CrossRef Medline

Makinson CD, Tanaka BS, Lamar T, Goldin AL, Escayg A (2014) Role of the hippocampus in Nav1.6 (Scn8a) mediated seizure resistance. Neurobiol Dis 68:16–25. CrossRef Medline

Malhotra JD, Kazen-Gillespie K, Hortsch M, Isom LL (2000) Sodium channel b subunits mediate homophilic cell adhesion and recruit ankyrin to points of cell-cell contact. J Biol Chem 275:11383–11388. CrossRef Medline

Marionneau C, Carrasquillo Y, Norris AJ, Townsend RR, Isom LL, Link AJ, Nerbonne JM (2012) The sodium channel accessory subunit Navbeta1 regulates neuronal excitability through modulation of repolarizing voltage-gated K(+) channels. J Neurosci 32:5716–5727. CrossRef Medline

Meadows LS, Malhotra J, Loukas A, Thyagarajan V, Kazen-Gillespie KA, Koopman MC, Kriegler S, Isom LL, Ragsdale DS (2002) Functional and biochemical analysis of a sodium channel $\beta$1 subunit mutation responsible for generalized epilepsy with febrile seizures plus type 1. J Neurosci 22:10699–10709. Medline

Moran O, Conti F (2001) Skeletal muscle sodium channel is affected by an epileptogenic $\beta$1 subunit mutation. Biochem Biophys Res Commun 282: 55–59. CrossRef Medline

Oakley JC, Kalume F, Yu FH, Scheuer T, Catterall WA (2009) Temperature- and age-dependent seizures in a mouse model of severe myoclonic epilepsy in infancy. Proc Natl Acad Sci U S A 106:3994–3999. CrossRef Medline

O'Malley HA, Isom LL (2015) Sodium channel beta subunits: emerging targets in channelopathies. Annu Rev Physiol 77:481–504. CrossRef Medline

Oyama F, Miyazaki H, Sakamoto N, Becquet C, Machida Y, Kaneko K, Uchikawa C, Suzuki T, Kurosawa M, Ikeda T, Tamaoka A, Sakurai T, Nukina N (2006) Sodium channel beta4 subunit: down-regulation and possible involvement in neuritic degeneration in Huntington's disease transgenic mice. J Neurochem 98:518–529. CrossRef Medline

Patino GA, Isom LL (2010) Electrophysiology and beyond: multiple roles of Na+ channel beta subunits in development and disease. Neurosci Lett 486:53–59. CrossRef Medline

Patino GA, Claes LR, Lopez-Santiago LF, Slat EA, Dondeti RS, Chen C, O'Malley HA, Gray CB, Miyazaki H, Nukina N, Oyama F, De Jonghe P, Isom LL (2009) A functional null mutation of SCN1B in a patient with Dravet syndrome. J Neurosci 29:10764–10778. CrossRef Medline

Patino GA, Brackenbury WJ, Bao Y, Lopez-Santiago LF, O'Malley HA, Chen C, Calhoun JD, Lafrenière RG, Cossette P, Rouleau GA, Isom LL (2011) Voltage-gated Na+ channel beta1B: a secreted cell adhesion molecule involved in human epilepsy. J Neurosci 31:14577–14591. CrossRef Medline

Racine RJ (1972) Modification of seizure activity by electrical stimulation: II. Motor seizure. Electroencephalogr Clin Neurophysiol 32:281–294. CrossRef Medline

Reid CA, Leaw B, Richards KL, Richardson R, Wimmer V, Yu C, Hill-Yardin EL, Lerche H, Scheffer IE, Berkovic SF, Petrou S (2014) Reduced dendritic arborization and hyperexcitability of pyramidal neurons in a Scn1b-based model of Dravet syndrome. Brain 137:1701–1715. CrossRef Medline

Rusconi R, Scalmani P, Cassulini RR, Giunti G, Gambardella A, Franceschetti S, Annesi G, Wanke E, Mantegazza M (2007) Modulatory proteins can rescue a trafficking defective epileptogenic Nav1.1 Na+ channel mutant. J Neurosci 27:11037–11046. CrossRef Medline

Scheffer IE, Berkovic SF (1997) Generalized epilepsy with febrile seizures plus: a genetic disorder with heterogeneous clinical phenotypes. Brain 120:479–490. CrossRef Medline

Scheffer IE, Harkin LA, Grinton BE, Dibbens LM, Turner SJ, Zielinski MA, Xu R, Jackson G, Adams J, Connellan M, Petrou S, Wellard RM, Briellmann RS, Wallace RH, Mulley JC, Berkovic SF (2007) Temporal lobe epilepsy and GEFS+ phenotypes associated with SCN1B mutations. Brain 130:100–109. Medline

Singh R, Scheffer IE, Crossland K, Berkovic SF (1999) Generalized epilepsy with febrile seizures plus: a common childhood-onset genetic epilepsy syndrome. Ann Neurol 45:75–81. CrossRef Medline

Tammaro P, Conti F, Moran O (2002) Modulation of sodium current in mammalian cells by an epilepsy-correlated beta 1-subunit mutation. Biochem Biophys Res Commun 291:1095–1101. CrossRef Medline

Wallace RH, Wang DW, Singh R, Scheffer IE, George AL Jr, Phillips HA, Saar K, Reis A, Johnson EW, Sutherland GR, Berkovic SF, Mulley JC (1998) Febrile seizures and generalized epilepsy associated with a mutation in the $Na^+$-channel beta1 subunit gene SCN1B. Nat Genet 19:366–370. CrossRef Medline

Wallace RH, Scheffer IE, Parasivam G, Barnett S, Wallace GB, Sutherland GR, Berkovic SF, Mulley JC (2002) Generalized epilepsy with febrile seizures plus: mutation of the sodium channel subunit SCN1B. Neurology 58: 1426–1429. CrossRef Medline

Wimmer VC, Reid CA, Mitchell S, Richards KL, Scaf BB, Leaw BT, Hill EL, Royeck M, Horstmann MT, Cromer BA, Davies PJ, Xu R, Lerche H, Berkovic SF, Beck H, Petrou S (2010) Axon initial segment dysfunction in a mouse model of genetic epilepsy with febrile seizures plus. J Clin Invest 120:2661–2671. CrossRef Medline

Wimmer VC, Harty RC, Richards KL, Phillips AM, Miyazaki H, Nukina N, Petrou S (2015) Sodium channel beta1 subunit localizes to axon initial segments of excitatory and inhibitory neurons and shows regional heterogeneity in mouse brain. J Comp Neurol 523:814–830. CrossRef Medline

Yu FH, Mantegazza M, Westenbroek RE, Robbins CA, Kalume F, Burton KA, Spain WJ, McKnight GS, Scheuer T, Catterall WA (2006) Reduced sodium current in GABAergic interneurons in a mouse model of severe myoclonic epilepsy in infancy. Nat Neurosci 9:1142–1149. CrossRef Medline